Journal of The Electrochemical Society, **166** (4) A787-A792 (2019)
0013-4651/2019/166(4)/A787/6/$38.00 © The Electrochemical Society

Optimal Condition of Solid-Electrolyte-Interphase Prepared by Controlled Prelithiation for High Performance Li-Ion Batteries

Dae In Lee,[1] Hyeon-Woo Yang,[1] Woo Seung Kang,[2] Jongsoon Kim,[1,z] and Sun-Jae Kim[1,z]

[1]*Department of Nanotechnology and Advanced Materials Engineering, Sejong University, Seoul 05006, Korea*
[2]*Department of Metallurgical and Materials Engineering, Inha Technical College, Incheon 22212, Korea*

The uneven formation of a solid-electrolyte interphase (SEI) in Li-ion batteries (LIBs) results in continuous electrolyte consumption and poor ionic conductivity, leading to degradation of the electrochemical performance. In this study, we report the optimal conditions for SEI formation to achieve enhanced electrochemical performance of a SiO_x anode in LIBs using a pre-lithiation under short-circuit-containing constant-resistance (PLSC) process. The SiO_x electrode prepared using the PLSC process delivers more outstanding cycle life (capacity retention of ~88.6% over 500 cycles) than that of an electrode prepared using the normal discharging process. Furthermore, PLSC process results in significantly improved power capability of SiO_x with a capacity retention of ~66.6% at 3 A g^{-1} (vs. the capacity measured at 0.1 A g^{-1}).
 [DOI: 10.1149/2.1201904jes]

Manuscript submitted December 12, 2018; revised manuscript received February 11, 2019. Published March 12, 2019.

Li-ion batteries (LIBs) have attracted great attention as one of the best energy storage systems (ESSs) because of their high energy density and power capability with stable cycle life.[1–3] Recently, the application range of LIBs has been extended from small devices such as laptops or cellphones to grid-scale ESSs such as electric vehicles. Because the gravimetric energy density of graphite-based energy materials typically used as anodes in LIBs is only ~372 mAh g^{-1}, the development of novel high-energy-density electrode materials is needed for further grid-scale application of LIBs.[4–7] However, most potential high-energy-density anode materials for LIBs, such as Si,[8,9] SnO_2,[10,11] Co_3O_4,[12,13] and other materials,[14,15] are based on a conversion or alloying reaction, which is accompanied by large volume change during charge/discharge. This large volume change results in poor cycle life due to pulverization of the anode materials and unwanted continuous formation of a solid-electrolyte interphase (SEI) that reduce the stable cycle life.[16–19] To improve the electrochemical performance of anode materials for LIBs, various approaches have been studied and reported.[20–26]

Recently, SiO_x has attracted great attention as a promising anode material for LIBs because of its large energy density resulting from the Li–Si alloying reaction and non-active SiO_2 buffer matrix, which prevents severe volume expansion during charge/discharge.[27–29] However, even though SiO_x exhibits high cycle performance in general, its initial coulombic efficiency remains as poor as those of other anode materials because of the irreversible capacity at initial discharge resulting from the SEI formation.[30–32] Surface coating is known to enable stable SEI formation with suppression of its growth, which can enhance the cyclability of anode materials for LIBs.[33,34] Moreover, several reports have shown that electrolyte additives can effectively improve the stability of the SEI at the electrode surface and reduce the irreversible capacity loss.[35,36] Thus, a fundamental understanding of the SEI and its relation to the electrochemical performance of LIBs is highly important.

Herein, we investigated the change of electrochemical performances of SiO_x depending on the accumulated SEI amounts into the electrode. Various SiO_x electrodes were prepared using a controlled pre-lithiation process that used an optimized circuit resistance for delicate control of the lithiation. During the initial discharge, it was verified that not only excess formation of the SEI but also the formation of a small amount of SEI results in poor electrochemical performance. This finding indicates that a suitable amount of SEI in the electrode can be used to prepare anode materials with optimal properties for LIBs. In particular, we discovered that the effect of the SEI on the electrochemical performance over the entire cycling process was mainly determined by the initial formation of the SEI in the electrode. Compared with a pristine SiO_x electrode, the SiO_x electrode prepared using the pre-lithiation under short-circuit-containing constant-resistance (PLSC) process exhibited an outstanding capacity retention of ~88.6% over 500 cycles with a high coulombic efficiency of ~99%. Furthermore, the power capability of the SiO_x electrode was highly enhanced by the PLSC process.

Experimental

Sample preparation.—The SiO_x composite powder for the anode materials was synthesized by solution reaction of $SiCl_4$ (99%, Wako Co.), benzene (99.5%, Daejung Co.), and ethylene glycol (EG, 99.9%, Samchun Co.). In the synthesis process, $SiCl_4$ and benzene were first stirred for 30 min; EG was then added with continuous stirring of the mixed solution. Benzene was used to promote the reaction between EG and $SiCl_4$. After the solution reaction, a white precursor was obtained. The SiO_x composite powder was finally obtained after heat-treatment of the white precursor at 725°C for 1 hour under vacuum condition.[37] Additionally, Supporting Figure S1 shows that the average particle size d_{50} of SiO_x is ~3.24 μm.

Electrochemistry characterization.—Electrodes were fabricated for the electrochemical evaluation. SiO_x samples (70 wt%) were mixed with deionized water (solvent), Super P (SP; 20%, TIMCAL Co.), and carboxy methyl cellulose (CMC; 10 wt%, Sigma Aldrich Co). The slurries were coated on copper foil and dried under vacuum at 80°C. A Nanoporosity Surface Area Analyzer which is made by Mirae incorporation was used for the electrode surface area and porosity measurements. Nitrogen was used as an absorbent gas. Brunnauer-Emmett-Teller (BET) software supplied by Nanoporosity Surface Area Analyzer was used for porosity calculations. As shown in the Supporting Figure S2, the porosity and BET-surface area of the electrode is 7.15 m^2 g^{-1} and 19.82 m^2 g^{-1}, respectively. Moreover, we compared the porosity and BET-surface area among several electrodes, and it was verified that the difference among each electrode is negligible. Coin-type cells (CR2032) were assembled in an Ar-filled glove box using Celgard 2400 as the separator. Li metal was used as the counter and reference electrodes, and 1.2 M $LiPF_6$ in a mixture of ethylene carbonate:dimethyl carbonate (3:7 v/v) + 3% vinylene carbonate was used as the electrolyte. The coin cells were charged and discharged between 0.01 and 1.5 V (vs. Li/Li^+) by applying various currents from 0.1 to 5 A g^{-1} at 25°C for electrochemical characterization. Two different discharging processes were used to verify the formation of the SEI in the electrodes, which was correlated to the initial irreversibility. The resistance was only applied at the pre-lithiation process (1st discharging process), and it was not used at the other charge/discharge cycles. After the PLSC process was finished, the cell was stabilized for 10 hours. Since then, the discharge/charge cycling process has been carried out under the same conditions as ND process. In addition, we

[z]E-mail: jongsoonkim@sejong.ac.kr; sjkim1@sejong.ac.kr

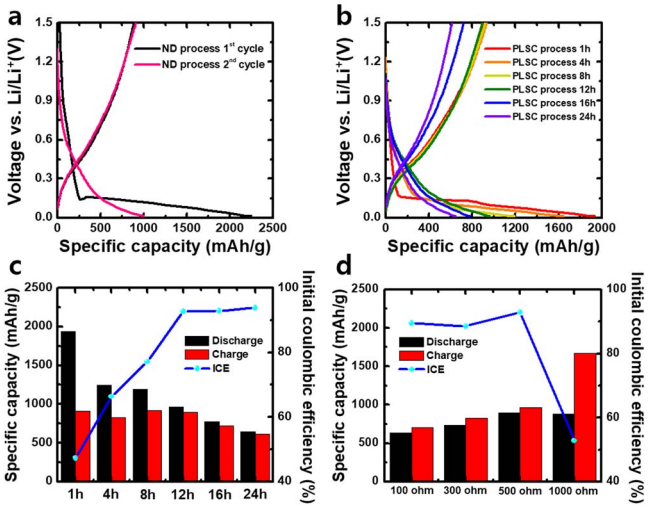

Figure 1. (a) 1st and 2nd charge–discharge profiles after ND process (current density of 100 mA g^{-1}). (b) 1st charge–discharge profiles after PLSC process with different charging times. Comparison of the specific capacity and ICE after PLSC process with (c) different discharge time when fixed resistance on 500 Ohm, (d) various resistance when fixed discharge time at 12 hours.

performed impedance analyses and constructed Nyquist plots in the frequency range of 1 MHz to 1 mHz with an ac amplitude of 10 mV.

Material characterization.—Chemical and structural analyses of the SEI formed by the normal discharging (ND) and PLSC processes were performed using X-ray photoelectron spectroscopy (XPS; Thermo VG U.K. K-alpha), field-emission scanning electron microscopy (FE-SEM; Hitachi S-4700), focused ion beam (FIB) milling (ZEISS crossbeam 540), and high-resolution transmission electron microscopy (HR-TEM; JEM-F200) and energy-dispersive X-ray spectroscopy (EDS) mapping.

Results and Discussion

To find the optimal condition of solid-electrolyte-interphase (SEI) by PLSC process, we controlled time and resistance. ND process and PLSC process were conducted in a Li-cell test room maintained at room temperature of 25°C. After the PLSC process was finished, the cell was stabilized for 10 hours. Since then, the discharge/charge cycling process has been carried out under the same conditions as ND process. Compared with the initial discharge capacity of SiO_x after the ND process, after the PLSC process, a lower initial discharge capacity and higher coulombic efficiency were observed (Figures 1a–1b). PLSC is the pre-lithiation process under short-circuit-containing constant-resistance for optimal formation of SEI in the electrode, which indicates that with increase of the PLSC process time, the electrode was more discharged. Thus, increase of the PLSC process time results in decrease of the specific discharge capacity of the electrode during the constant-current discharge process after the PLSC process. When the PLSC process time was increased, the initial reversibility at the constant-current charge/discharge process after the PLSC process became better, however, after too much PLSC process time, the initial reversibility became worse. (Figure 1c) Thus, the best PLSC process time was 12 hours. Moreover, we performed the PLSC process using various resistances of 100, 300, 500, and 1000 Ohm over 12 hours. It was verified that initial Coulombic efficiency (ICE) of the electrode using 500 Ohm resistance for the PLSC process was more outstanding than those using the other resistances. (Figure 1d) Based on these results, we confirmed that for the optimal PLSC process, 500 Ohm and 12 hours should be required to satisfy both the capacity and the ICE, which indicates that SEI formation and prelithiation at the SiO_x electrode were well controlled using the PLSC process. In addition, a comparison of the coulombic efficiency and charge/discharge capacity over 5 cycles for the normally discharged pristine SiO_x and the SiO_x after 12 hours of the PLSC is presented in Supporting Figure S3. Loading-mass of the electrode was ~0.227 mg cm^{-2}, and the difference of loading mass among the used electrodes were negligible. The initial discharging capacities of electrodes treated with ND process and PLSC are 1978 mAh g^{-1} (0.449 mAh cm^{-2}) and 1109 mAh g^{-1} (0.252 mAh cm^{-2}), respectively. Whereas the coulombic efficiency of the pristine SiO_x reached ~95% after 5 cycles, only 2 cycles were required to reach this level for the SiO_x after 12 hours of the PLSC process. This finding indicates that the SEI formation, which determines the coulombic efficiency of the initial cycles, was significantly affected by the PLSC process. In addition, it was verified through SEM-EDS analyses that the molar ratio of Si and O in the SiO_x electrode was 1:1.64 (Supporting Table S1), and the molar mass of the active material in the electrode is ~54.3245 g mol^{-1}. Thus, we converted the capacity measured during PLSC to the amounts of Li ions (Supporting Figure S4). Moreover, we recorded the variation of current density as function of the PLSC process time (Supporting Figure S5). The current density at initial 10 seconds of the PLSC process was 2940 mA g^{-1}, and then after 1 minute, the current density was sharply decreased to 500 mA g^{-1}. After the PLSC process time of 4 hours and 12 hours, the measured current densities were 285 mA g^{-1} and 170 mA g^{-1}. On the other hand, during the ND process, the current density was constantly retained to 100 mA g^{-1}. Figure 2 shows the morphological change of the SiO_x electrode as a function of the PLSC processing time. Because PLSC is the pre-lithiation process under short-circuit-containing constant-resistance, SEI was formed around surface of the particles in the electrode. Thus, with increase of the PLSC process time, the electrode was more filled with the SEI, which implies that with SEI formation under the PLSC process, vacancies and boundaries that prevent Li-ion diffusion disappeared at the electrode. It was reported that the SiO_x morphology was well retained during charge/discharge process because of existence of non-active SiO_2 buffer matrix that could prevent severe volume expansion arising from Li-Si alloying reaction.[8,38] Thus, it was supposed that the SEI formed after the PLSC process might keep its original shape despite charge/discharge process of SiO_x, which implies that the initial formation of SEI by the PLSC process might determine the electrochemical performances of the SiO_x electrode. (Supporting Figure S6) However, after 12 hours of the PLSC process, too much SEI was stacked at the electrode, and then SEI cracked with formation of many boundaries at the electrode, which indicates the negative effect of excessive PLSC processing. It was observed through the cross-section SEM images that thickness of the SEI formed on the electrode surface becomes thicker as the discharging time increases. As shown in Supporting Figure S7, thickness of the SEIs after the PLSC process for 12 hours and 24 hours are ~78 nm and ~154 nm. We supposed that increase of the SEI thickness may result from increase of accumulated Li amount in the electrode during the PLSC process. When too much Li were accumulated in the electrode, the SEI may be damaged and cracked, which causes degradation of electrochemical performances of the electrodes. Additionally, TEM analysis revealed SiO_x particles homogenously encapsulated by the SEI. Furthermore, as observed in Figure 3, compounds composed of P, F, C, and O, which are known as the main elements of the SEI, were closely packed among the SiO_x particles with sizes greater than 1μm.

The improvement in the Li-ion diffusion through the electrode closely packed with the SEI using the PLSC process was confirmed by electrochemical impedance spectroscopy (EIS) measurements performed after initial discharge over the frequency range of 1 MHz to 1 mHz with an ac amplitude of 10 mV. The Nyquist plots of the PLSC-processed electrodes consisted of a semicircle at high frequency and a straight line at low frequency.[39,40] The diameter of the semicircle is related to the charge-transfer resistance arising from the reaction occurring at the electrode–electrolyte interface.[41] As shown in Figure 4a, with increasing PLSC processing time, the charge-transfer resistance of the SiO_x electrode decreased until after 12 hours, after 12 hours it increased. This finding indicates that the PLSC process for 12 hours is

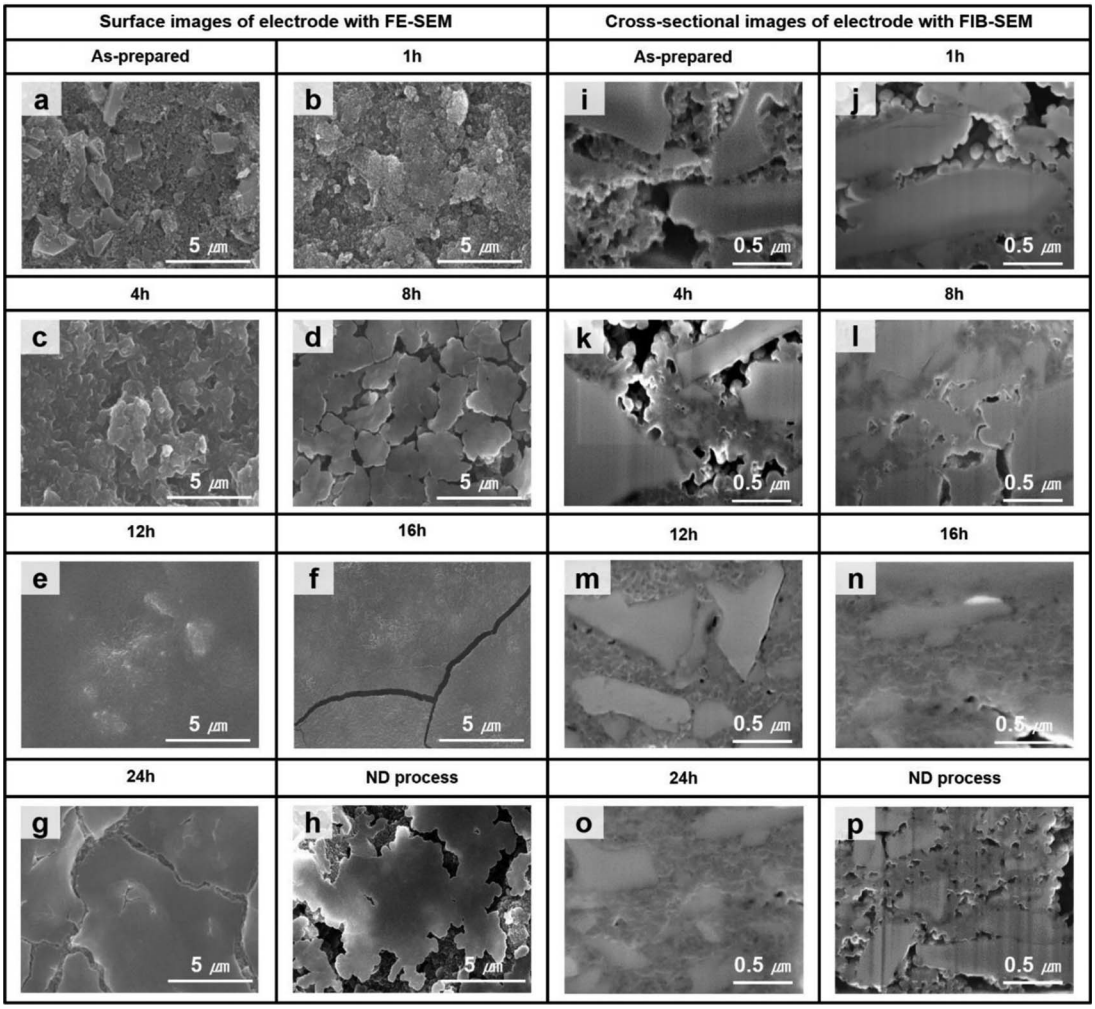

Figure 2. SEM micrographs of as-prepared electrode (a) surface and (i) cross-section. (b–g) SEM micrographs of electrode surface after discharge using different charging times for PLSC process. (j–o) FIB–SEM micrographs of electrode cross-sections after discharge using different charging times for PLSC process. SEM images of electrode (h) surface and (p) cross-section after discharge for ND process.

optimal for the uniform formation of the SEI with minimized vacancies and boundaries in the SiO_x electrode. In addition, we verified that the ionic conductivity of the SiO_x electrode was significantly improved through control of the PLSC process. The Li-ion diffusion coefficient (D_{Li}^+) in the SiO_x electrode was calculated using Equation 1:

$$D_{Li}^{+} = R^2T^2/2A^2n^4F^4C^2\sigma^2 \quad [1]$$

where σ_w is the Warburg impedance coefficient (Figure 4b), R is the gas constant, T is the temperature, A is the surface area, n is the number of electrons participating in the reaction, F is the Faraday constant, and C is the maximum ion concentration.[42,43]

The electrode after 12 hours of the PLSC process delivered more than four-times higher ionic conductivity than that after 1 hour of the PLSC process, which indicates that close packing of the SiO_x particles with a highly ionic conductive SEI enables high enhancement of the electrochemical performance of the SiO_x electrode. It was reported that SEI exhibits high ionic conductivity[31,38] which implies lowering charge transfer resistance of the electrode by that well-formed SEI. However, existence of vacancies and boundaries at the electrode may prevent fast Li^+ insertion/extraction from surface of the electrode to inner part, which may not provide sufficient Li-ion diffusion pathways. Thus, we supposed that the electrode with well-formed SEI through optimal PLSC process exhibited lower charge transfer resistance than the others. Table I and Figures 4c–4d show that the D_{Li}^+ value at the SiO_x electrode after 12 hours of the PLSC process is ~39 times faster than that after the ND process. Thus, we confirmed that uniform SEI formation by the PLSC process provides fast Li^+ ionic diffusion paths connecting each SiO_x particle in the electrode, which may result in the highly improved electrochemical performance of the SiO_x electrode. Additionally, it has been known that the front semicircle observed at the impedance means the resistance between the electrolyte and the electrode and the semicircle that appears afterward indicates the resistance of the electrode. In case of our EIS analyses, the semicircle associated with the SEI resistance was hardly observed (Figure 4a).

Table I. R_{el}, R_{ct}, σ_w, and Li-ion diffusion coefficients of PLSC and ND processes.

	PLSC 1 h	PLSC 4 h	PLSC 8 h	PLSC 12 h	PLSC 16 h	PLSC 24 h	ND process
R_{el}/Ω	1.312	0.916	1.412	1.144	1.066	0.830	3.565
R_{ct}/Ω	412.19	306.93	286.37	238.85	279.63	290.62	426.084
$\sigma_w/\Omega\ s^{-1/2}$	14.08	12.31	11.11	6.66	6.78	9.60	132.8
$D_{Li}^+/cm^2\ s^{-1}$	1.275×10^{-12}	1.668×10^{-12}	2.051×10^{-12}	5.697×10^{-12}	5.497×10^{-12}	2.742×10^{-12}	1.433×10^{-13}

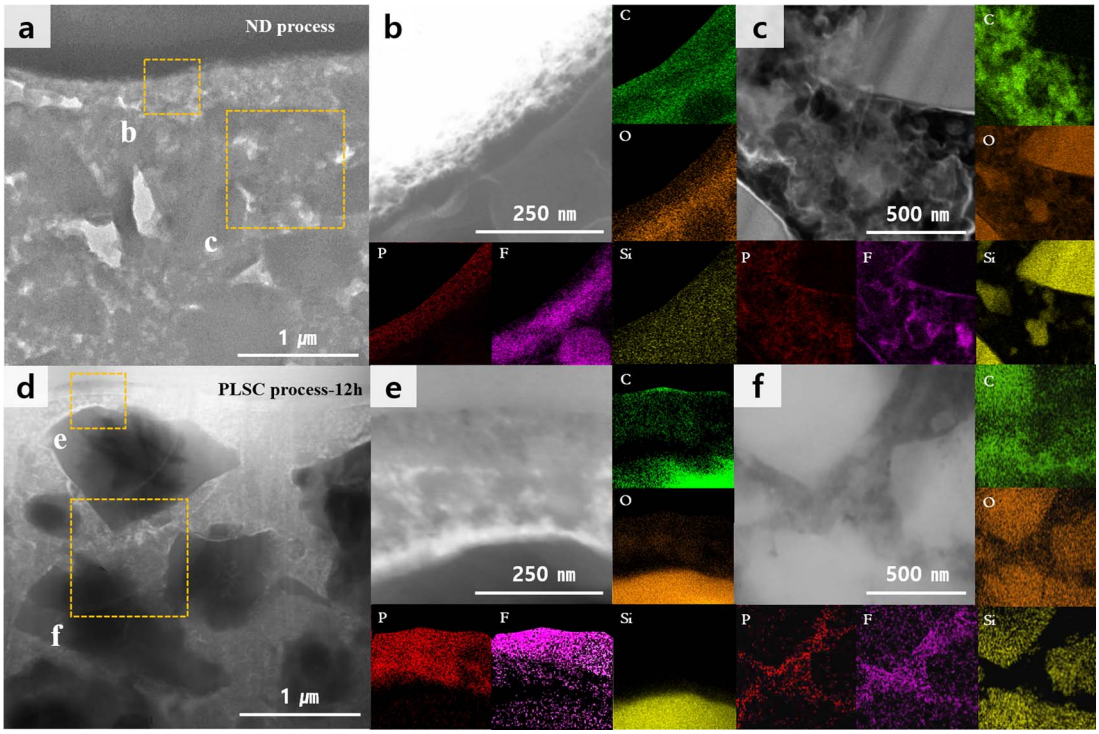

Figure 3. HR-TEM characterization of electrodes. (a)–(d) TEM images of electrode discharged using ND and PLSC (12 hours) processes. (b)–(e) Surfaces of different discharged electrodes using ND and PLSC (12 hours) processes. (c)–(f) Cross-sections of different discharged electrodes using ND and PLSC (12 hours) process.

We performed the EIS analyses several times to observe the resistance associated with the SEI, however, we could not detect the meaningful information on the SEI resistance. Thus, it was supposed that the resistance arising from the SEI might be negligible because the resistance of the electrode is much larger than that of the SEI.

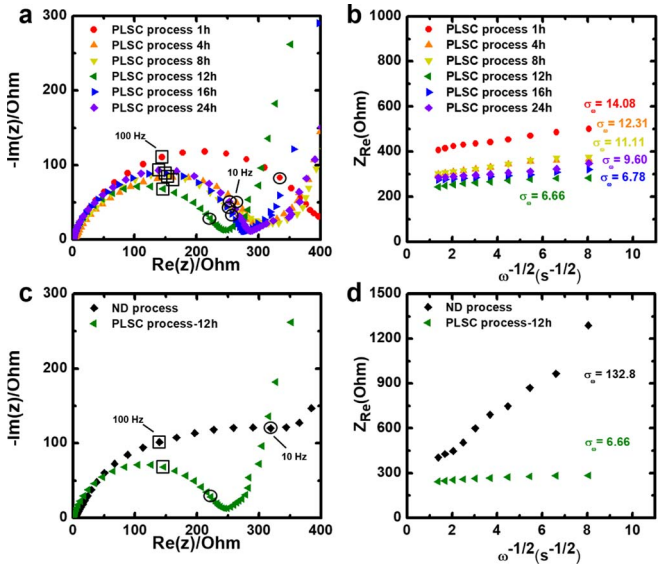

Figure 4. (a) Electrochemical impedance spectra of Nyquist plots in high-frequency range for PLSC process with different discharging times. (b) Comparison of ion conductivity with Warburg impedance coefficients of PLSC process for different discharging times. (c) Electrochemical impedance spectra of Nyquist plots in the high-frequency range of ND and PLSC (12 hours) processes. (d) Comparison of ion conductivity with Warburg impedance coefficients of ND and PLSC (12 hours) processes.

Detailed information on the ionic bonding of the SEI layers was verified using XPS analyses. As shown in Figure 5a, after the PLSC process, the Si 2p peak was observed at ∼102 eV, which indicates the formation of lithium silicates (Li_xSiO_y). The existence of Li_xSiO_y was also verified in the O 1s spectra (Figure 5b). Whereas the O 1s peak for SiO_x after the ND process appeared at ∼533 eV, corresponding to SiO_2, the O 1s peak was shifted to ∼531.4 eV after the PLSC process, which is indicative of the presence of Li_xSiO_y. These results agree well with a previous report.[44] Figure 5c presents the C 1s spectra of the SiO_x electrodes after the ND and PLSC processes. The C–C (∼ 285.0 eV) and C–O (∼287.0 eV) bonds

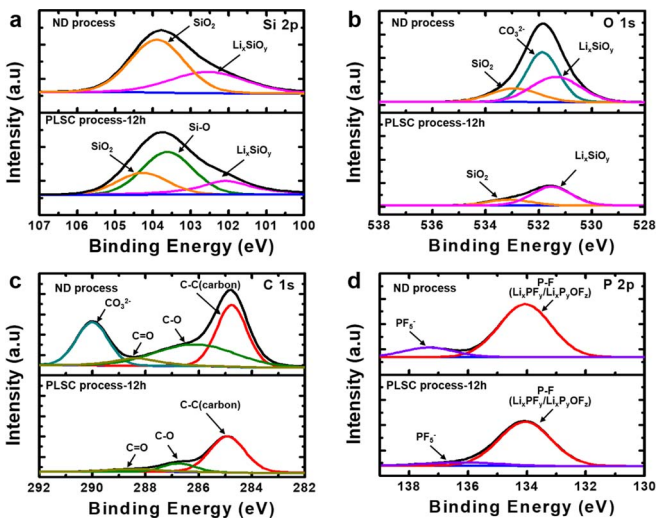

Figure 5. XPS spectra showing (a) Si 2p, (b) O 1s, (c) C 1s, and (d) P 2P peaks after ND and PLSC (12 hours) processes.

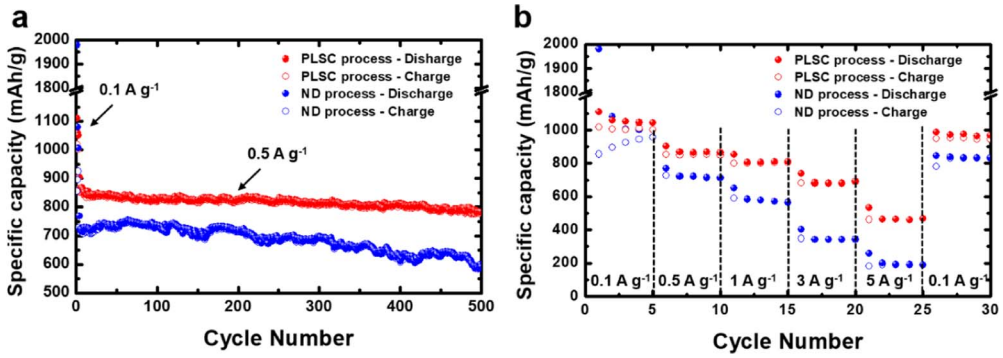

Figure 6. (a) Long-life cycling performance of electrode after ND and PLSC processes during 500th cycle and coulombic efficiency (1st–3rd pre-cycle current density: 0.1 A g^{-1}, after 3rd cycle current density: 0.5 A g^{-1}). (b) Cycling performance at different rates from 0.1C to 5C.

originated from the carbon and binder in the electrode.[45–47] After the ND process, the CO_3^{2-} bond corresponding to Li_2CO_3, which is known to be an irreversible product formed during initial discharging, was strongly observed at ~290.3 eV, and the C=O bond was also detected at ~289.1 eV.[37,48] However, after the PLSC process, the peaks related to CO_3^{2-} and C=O bonds were hardly detected. Furthermore, whereas the PF_5^- bond (~137.2 eV), which is known as a component that causes deterioration of the electrochemical performance of the electrode,[49] was detected in the P 2p spectrum of the SiO_x electrode after the ND process, it was not observed after the PLSC process (Figure 5d).

The optimally formed SEI layer at the electrode using the PLSC process enables highly enhanced electrochemical performance of SiO_x. The electrodes were tested at a current density of 500 mA g^{-1} in the voltage range of 0.01–1.5 V. As observed in Figure 6a, the SiO_x electrode after the PLSC process exhibited more outstanding cycle performance than that after the ND process.

Over 500 cycles, up to 88.6% of the initial capacity of the SiO_x electrode was maintained after the PLSC process. Furthermore, it was verified that the power capability of the SiO_x electrode was highly improved by the PLSC process (Figure 6b). Whereas the SiO_x electrode after the ND process only deliver ~40.4% capacity retention at 3 A g^{-1} (vs. the capacity measured at 0.1 A g^{-1}), its capacity after the PLSC process measured at 3 A g^{-1} was maintained up to ~66.6% of that measured at 0.1 A g^{-1}. The differences in the SEI formation between the ND and PLSC processes are summarized in Figure 7. The well-controlled SEI after the PLSC process resulted in highly enhanced electrochemical performance of the SiO_x electrode, including an excellent cycle life, high coulombic efficiency, and outstanding power capability.

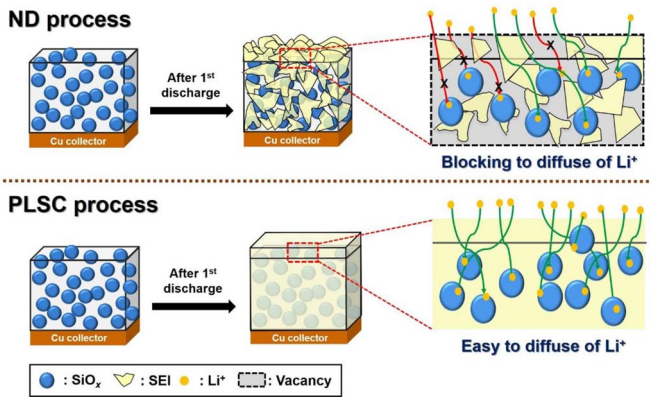

Figure 7. Schematic illustration of SEI formed using two different discharging processes.

Conclusions

We demonstrated that optimal formation of the SEI layer at the electrode using a simple PLSC process enables highly enhanced electrochemical performance of a SiO_x electrode as a promising anode for LIBs. By controlling the reaction time of the PLSC process, SEI layers were successfully formed not only on the surface of the electrode but also in the electrode without vacancies and boundaries, resulting in outstanding electrochemical performance of the SiO_x electrode. Over 500 cycles, the SiO_x electrode after the PLSC process exhibited a highly stable cycle life with ~88.6% capacity retention compared with the initial capacity. Furthermore, at 0.5 A g^{-1}, the electrode delivered a capacity of ~876 mAh g^{-1}, corresponding to ~80% of the capacity measured at 0.1 A g^{-1}. We believe that our work provides important insight for the commercialization of not only SiO_x electrodes but also other conversion-based/alloying-based anodes for LIBs.

Acknowledgment

This work was supported by the National Research Foundation of Korea(NRF) grant funded by the Korea government (MSIP; Ministry of Science, ICT & Future Planning) (NRF-2015M3D1A1069713) and (NRF-2016R1A2B4014521).

ORCID

Dae In Lee https://orcid.org/0000-0001-8204-0572
Hyeon-Woo Yang https://orcid.org/0000-0003-3863-9363
Jongsoon Kim https://orcid.org/0000-0002-7651-5516
Sun-Jae Kim https://orcid.org/0000-0002-7908-7086

References

1. R. A. Huggins and W. D. Nix, *Ionics*, **6**, 57 (2000).
2. B. Dunn, H. Kamath, and J. M. Tarascon, *Science*, **334**, 928 (2011).
3. M. Armand and J. M. Tarascon, *Nature*, **451**, 652 (2008).
4. M. Winter, J. O. Besenhard, M. E. Spahr, and P. Novak, *Adv. Mater.*, **10**, 725 (1998).
5. H. Wu and Y. Cui, *Nano Today*, **7**, 414 (2012).
6. P. Poizot, S. Laruelle, S. Grugeon, L. Dupont, and J. M. Tarascon, *Nature*, **407**, 496 (2000).
7. M. N. Obrovac and V. L. Chevrier, *Chem. Rev.*, **114**, 11444 (2014).
8. H. W. Yang, H. Y. Park, H. G. Lee, W. S. Kang, and S. J. Kim, *ACS Omega*, **2**, 3518 (2017).
9. X. H. Liu, H. Zheng, L. Zhong, S. Huan, K. Karki, L. Q. Zhang, Y. Liu, A. Kushima, W. T. Liang, J. W. Wang, J. H. Cho, E. Epstein, S. A. Dayeh, S. T. Picraux, T. Zhu, J. Li, J. P. Sullivan, J. Cumings, C. S. Wang, S. X. Mao, Z. Z. Ye, S. L. Zhang, and J. Y. Huang, *Nano Lett.*, **11**, 3312 (2011).
10. X. S. Zhou, L. J. Wan, and Y. G. Guo, *Adv. Mater.*, **25**, 2152 (2013).
11. X. Wang, X. Q. Cao, L. Bourgeois, H. Guan, S. M. Chen, Y. T. Zhong, D. M. Tang, H. Q. Li, T. Y. Zhai, L. Li, Y. Bando, and D. Golberg, *Adv. Funct. Mater.*, **22**, 2682 (2012).
12. Z. S. Wu, W. C. Ren, L. Wen, L. B. Gao, J. P. Zhao, Z. P. Chen, G. M. Zhou, F. Li, and H. M. Cheng, *ACS Nano*, **4**, 3187 (2010).
13. Y. G. Li, B. Tan, and Y. Y. Wu, *Nano Lett.*, **8**, 265 (2008).
14. Y. Yu, C. H. Chen, J. L. Shui, and S. Xie, *Angew. Chem.-Int. Edit.*, **44**, 7085 (2005).

15. W. J. Zhang, *J. Power Sources*, **196**, 13 (2011).
16. Y. Jin, B. Zhu, Z. D. Lu, N. Liu, and J. Zhu, *Adv. Energy Mater.*, **7**, 17 (2017).
17. M. T. McDowell, I. Ryu, S. W. Lee, C. M. Wang, W. D. Nix, and Y. Cui, *Adv. Mater.*, **24**, 6034 (2012).
18. A. S. Arico, P. Bruce, B. Scrosati, J. M. Tarascon, and W. Van Schalkwijk, *Nat. Mater.*, **4**, 366 (2005).
19. M. R. Zamfir, H. T. Nguyen, E. Moyen, Y. H. Lee, and D. Pribat, *J. Mater. Chem. A*, **1**, 9566 (2013).
20. J. Xie, X. G. Yang, S. Zhou, and D. W. Wang, *ACS Nano*, **5**, 9225 (2011).
21. M. Y. Ge, J. P. Rong, X. Fang, A. Y. Zhang, Y. H. Lu, and C. W. Zhou, *Nano Res.*, **6**, 174 (2013).
22. L. David, R. Bhandavat, U. Barrera, and G. Singh, *Nat. Commun.*, **7**, 10 (2016).
23. B. Wang, X. L. Li, X. F. Zhang, B. Luo, M. H. Jin, M. H. Liang, S. A. Dayeh, S. T. Picraux, and L. J. Zhi, *ACS Nano*, **7**, 1437 (2013).
24. X. H. Liu, J. Zhang, W. P. Si, L. X. Xi, B. Eichler, C. L. Yan, and O. G. Schmidt, *ACS Nano*, **9**, 1198 (2015).
25. R. Deshpande, Y. T. Cheng, and M. W. Verbrugge, *J. Power Sources*, **195**, 5081 (2010).
26. M. Zhou, T. W. Cai, F. Pu, H. Chen, Z. Wang, H. Y. Zhang, and S. Y. Guan, *ACS Appl. Mater. Interfaces*, **5**, 3449 (2013).
27. E. Park, M. S. Park, J. Lee, K. J. Kim, G. Jeong, J. H. Kim, Y. J. Kim, and H. Kim, *ChemSusChem*, **8**, 688 (2015).
28. Y. M. Ju, J. A. Tang, K. Zhu, Y. Meng, C. Z. Wang, G. Chen, Y. J. Wei, and Y. Gao, *Electrochim. Acta*, **191**, 411 (2016).
29. W. J. Wu, J. Shi, Y. H. Liang, F. Liu, Y. Peng, and H. B. Yang, *Phys. Chem. Chem. Phys.*, **17**, 13451 (2015).
30. K. Yasuda, Y. Kashitani, S. Kizaki, K. Takeshita, T. Fujita, and S. Shimosaki, *J. Power Sources*, **329**, 462 (2016).
31. P. Verma, P. Maire, and P. Novak, *Electrochim. Acta*, **55**, 6332 (2010).
32. D. Aurbach, *J. Power Sources*, **89**, 206 (2000).
33. C. H. Gao, H. L. Zhao, P. P. Lv, C. M. Wang, J. Wang, T. H. Zhang, and Q. Xia, *J. Electrochem. Soc.*, **161**, A2216 (2014).
34. H. Wu, G. Chan, J. W. Choi, I. Ryu, Y. Yao, M. T. McDowell, S. W. Lee, A. Jackson, Y. Yang, L. B. Hu, and Y. Cui, *Nat. Nanotechnol.*, **7**, 309 (2012).
35. S. S. Zhang, *J. Power Sources*, **162**, 1379 (2006).
36. L. B. Chen, K. Wang, X. H. Xie, and J. Y. Xie, *J. Power Sources*, **174**, 538 (2007).
37. H. W. Yang, N. Kang, S. T. Myung, J. Kim, and S. J. Kim, *J. Electrochem. Soc.*, **165**, A1247 (2018).
38. T. Chen, J. Wu, Q. L. Zhang, and X. Su, *J. Power Sources*, **363**, 126 (2017).
39. Z. Q. Jiang, B. Pei, and A. Manthiram, *J. Mater. Chem. A*, **1**, 7775 (2013).
40. L. A. Geddes, *Chemical Instrumentation*, **4**, 157 (1972).
41. Y. Tan, K.-W. Wong, and K. M. Ng, *Small*, 13 (2017).
42. H.-W. Yang, D. I. Lee, N. Kang, J.-K. Yoo, S.-T. Myung, J. Kim, and S.-J. Kim, *J. Power Sources*, **400**, 613 (2018).
43. S. Li, X. Cao, C. N. Schmidt, Q. Xu, E. Uchaker, Y. Pei, and G. Cao, *J. Mater. Chem. A*, **4**, 4242 (2016).
44. H. J. Kim, S. Choi, S. J. Lee, M. W. Seo, J. G. Lee, E. Deniz, Y. J. Lee, E. K. Kim, and J. W. Choi, *Nano Lett.*, **16**, 282 (2016).
45. D. V. Novikov, E. Y. Evschik, V. I. Berestenko, T. V. Yaroslavtseva, A. V. Levchenko, M. V. Kuznetsov, N. G. Bukun, O. V. Bushkova, and Y. A. Dobrovolsky, *Electrochim. Acta*, **208**, 109 (2016).
46. P. Lu, C. Li, E. W. Schneider, and S. J. Harris, *J. Phys. Chem. C*, **118**, 896 (2014).
47. D. E. Arreaga-Salas, A. K. Sra, K. Roodenko, Y. J. Chabal, and C. L. Hinkle, *J. Phys. Chem. C*, **116**, 9072 (2012).
48. H. Yamamura, K. Nobuhara, S. Nakanishi, H. Iba, and S. Okada, *J. Ceram. Soc. Jpn.*, **119**, 855 (2011).
49. J. Kim, J. G. Lee, H. S. Kim, T. J. Lee, H. Park, J. H. Ryu, and S. M. Oh, *J. Electrochem. Soc.*, **164**, A2418 (2017).